International Journal of Energy and Environmental Engineering
a SpringerOpen Journal

ORIGINAL RESEARCH Open Access

# Analysis of free and forced convection in airflow windows using numerical simulation of heat transfer

Mohammad Ghadimi[1*], Hossein Ghadamian[1], Aliasghar A Hamidi[2], Farivar Fazelpour[3] and Mehdi A Behghadam[4]

**Abstract**

The present paper describes a two-dimensional finite volume numerical simulation of flow and heat transfer in airflow windows by free and forced convection techniques. The governing equations are the fully elliptic, Reynolds-averaged Navier–Stokes equations. The simple algorithm is employed to correct the pressure term. The second-order upwind scheme is used to discretize the convection terms. The ($k$-$\epsilon$/RNG) turbulence model is applied for the flow simulation. The mesh used is the body-fitted, multi-plane grid system. Results on the variations of velocity and temperature profiles with geometrical parameters, at different temperature and velocity, for heat transfer by free and forced convection techniques are presented. Comparisons of the present results on temperature distribution for forced convection and for free convection with the available experimental forced convection data indicate that the airflow-influenced forced convection methods are considerably enhanced.

**Keywords:** Advanced envelope, Airflow window, Building energy simulation, Energy performance, Fenestration, Office building, Solar energy, Wind

## Background

Improvement of building performance energy can be achieved by using airflow windows. Airflow windows in buildings are used to improve the indoor thermal comfort and/or reduce the energy use of air-conditioning systems. The airflow window is also an invention to improve the thermal comfort and reduce energy costs. It consists of a double window construction with an air cavity in between. Nowadays, the outside window is mostly a double-glazed window, and the inner window is a single glass leaf. On the bottom of the airflow cavity, exhaust air ventilation will be extracted out of the room and transported through the cavity to the exhaust duct, as can be seen in Figure 1. This results in less temperature difference between the inside glass surface and the room. This requires choosing a suitable heat transfer method to prevent missing energy in buildings. The mechanically ventilated variants include an airflow window and a supply-air window. The airflow window is a popular solution in fully conditioned office buildings.

The first studies on airflow windows were published in the 1950s in Scandinavia (Brandle and Boehm [1]; Ripatti [2]; Park et al. [3]). The issue was to improve the energy efficiency and the thermal comfort of residential fenestration. In 1957, the first patent related to airflow windows was filed in Sweden. In 1967, the EKONO Company built the first office building equipped with airflow windows in Helsinki, Finland (Brandle and Boehm [1]; Park et al. [3]).

The spirit for further development is to be found in the energy crises of 1973 and 1979. Suddenly, energy efficiency and thermal comfort were no longer an exclusive issue for Nordic climates. Experimental data for a Japanese building with an airflow window is available from Baker et al. [4], Ziller [5] and Busselen and Mattelaer [6]. Tracer gas techniques make it possible to determine the airflow rate in both naturally and mechanically ventilated active envelopes without interference with the driving forces. Busselen and Mattelaer [6], however, point out that it is difficult to illustrate the highly

* Correspondence: m.ghadimi@riau.ac.ir
[1]Department of Energy Engineering, Science and Research Branch, Islamic Azad University, P.O. Box 147789385, Tehran, Iran
Full list of author information is available at the end of the article

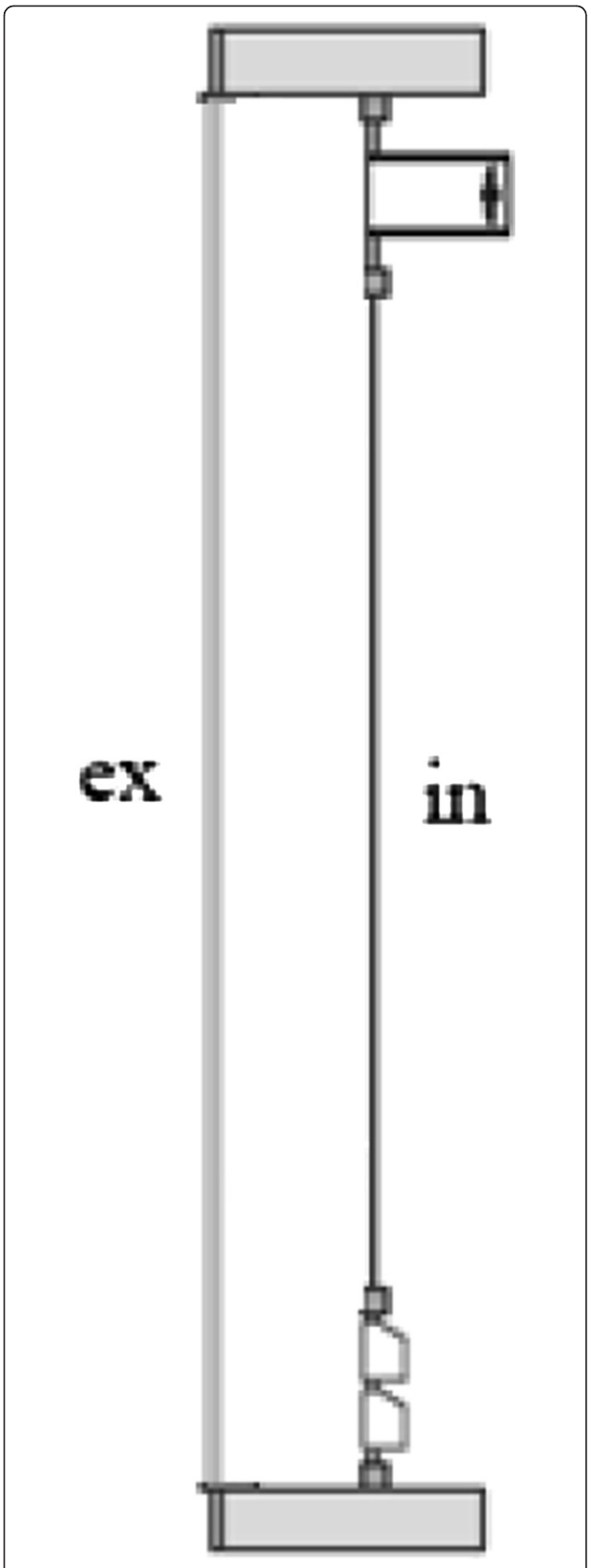


**Figure 1** Experimental model of an airflow window.

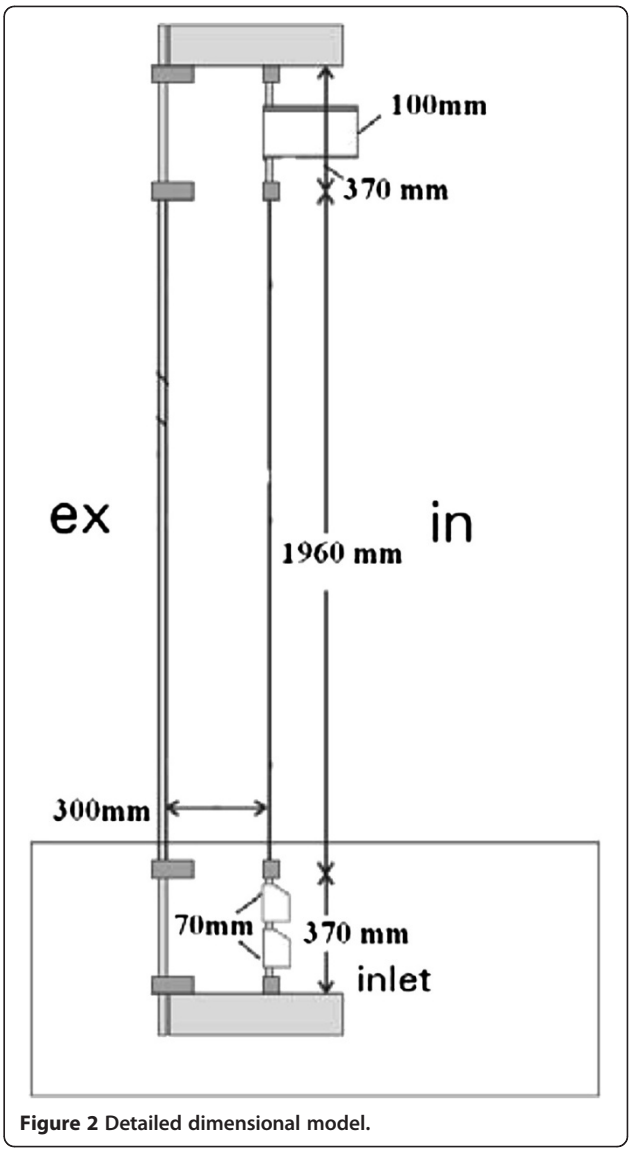


**Figure 2** Detailed dimensional model.

fluctuating airflow rate accurately with the constant emission technique. The same conclusions could be drawn from the measurements at the Postcheque building.

## Methods

### Governing equations

The time-averaged fully elliptic, Reynolds-averaged Navier–Stokes (RANS) equations governing the motion of an incompressible, steady and constant property flow are expressed in a general form as follows [7]. The conservation of mass, momentum and energy is defined in Equations 1, 2 and 3, respectively.

$$\frac{\partial(\rho u_j)}{\partial x_j} = 0 \tag{1}$$

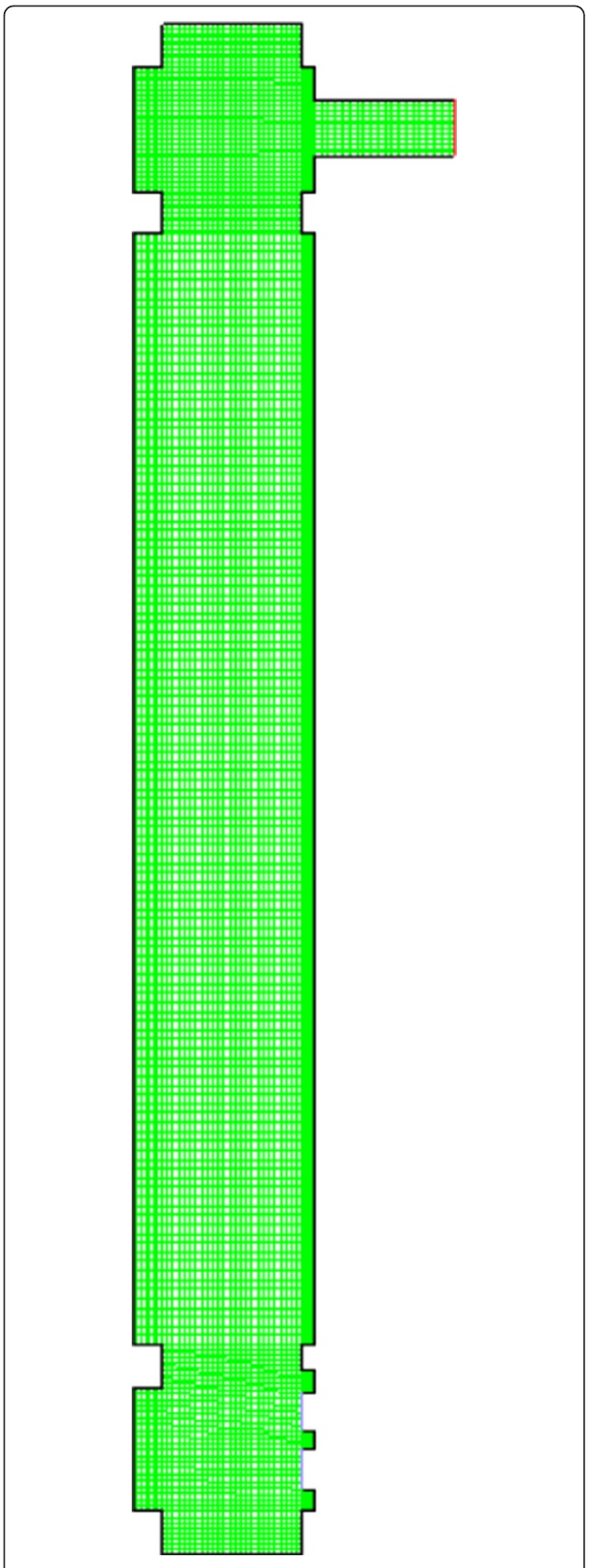

**Figure 3** Structured mesh for model.

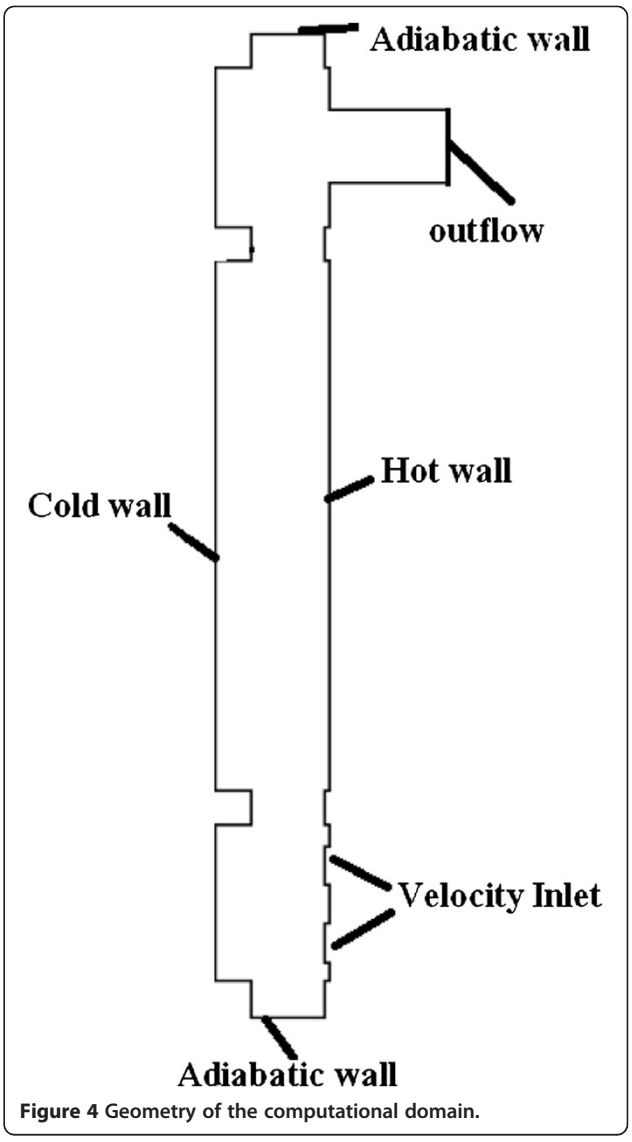


**Figure 4** Geometry of the computational domain.

where $\rho$ is density and $u$ is velocity vector.

$$\frac{\partial(\rho u_i u_j)}{\partial x_j} = -\frac{\partial P}{\partial x_j} + \frac{\partial}{\partial x_j}\left[(\mu + \mu_t)\frac{\partial u_j}{\partial x_j}\right] \tag{2}$$

where $P$, $\mu$ and $\mu_t$ are static pressure, laminar viscosity and turbulent eddy viscosity, respectively.

$$\frac{\partial(\rho u_i T)}{\partial x_i} = \frac{\partial}{\partial x_i}\left[\left(\frac{\mu}{\mathrm{Pr}} + \frac{\mu_t}{\mathrm{Pr}_t}\right)\frac{\partial T}{\partial x_j}\right] \tag{3}$$

where Pr and $\mathrm{Pr}_t$ are the molecular and turbulent Prandtl numbers, respectively. The proper choice of a turbulence model is of great importance, and it depends on many factors such as the flow physics, the required level of accuracy and the available computational resources. The ($k$-$\epsilon$/Renormalization group (RNG)) turbulence model [7] is based on the model (RNG)

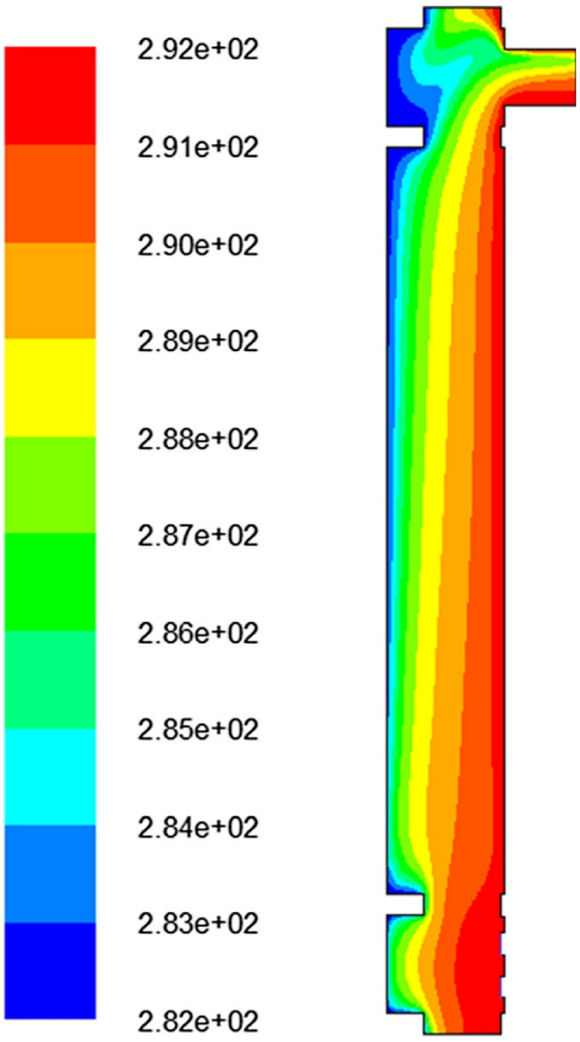


**Figure 5** Temperature distribution in the airflow window (present simulation).

equations for the turbulence kinetic energy, $k$, and its dissipation rate, $\epsilon$. The turbulence kinetic energy and its rate of dissipation are obtained from the following transport equations.

$$\frac{\partial}{\partial x_i}(\rho k u_i) = \frac{\partial}{\partial x_i}\left(\Gamma_k \frac{\partial k}{\partial x_j}\right) + G_k - Y_k \tag{4}$$

$$\frac{\partial}{\partial x_i}(\rho \epsilon u_i) = \frac{\partial}{\partial x_j}\left(\Gamma_\epsilon \frac{\partial \epsilon}{\partial x_j}\right) + G_\epsilon - Y_\epsilon + D_\epsilon \tag{5}$$

In these equations, $G_k$ represents the generation of turbulence kinetic energy due to mean velocity gradients. $Y_k$ represents the contribution of the fluctuating dilatation in compressible turbulence to the overall dissipation rate. The relevant boundary conditions, on the basis of Baker et al.'s [4] experimental work, are outlined in one of the following sections. In the RNG model, diffusion in $k$ and $\epsilon$ equations appears as:

$$(\mu + \mu_t) \times \alpha \tag{6}$$

while in the standard $k$-$\epsilon$ model, it is given by

$$\mu + \mu_t/\mathrm{Pr} \tag{7}$$

For the new implementation, a UDF is needed to define a Prandtl number, Pr, as

$$\mathrm{Pr} = \mu_t/((\mu + \mu_t) \times \alpha - \mu) \tag{8}$$

in order to achieve the same implementation as the original RNG model.

### Flow geometry

Figure 2 depicts a schematic view of the present airflow window model. It is similar in concept to Baker et al.'s [4] experimental model (see Figure 1). It comprises an inlet region, an outlet region and a main channel airflow. The airflow stream enters through the inlet region into the main channel airflow when it flows along the chamber, eventually flowing out through the outlet region. The main chamber is a rectangular cross section with a width equal to 300 mm and a height equal to 2,700 mm, the inlet vent has two equal widths, 70 mm, and the outlet region has width equal to 10 mm (see Figure 2). The airflow enters the channel at a rate of $G_i = 110$ m$^3$/h [8]. The origin of the coordinate system is positioned at the corner of the model.

### Grid generation

Computational fluid dynamics (CFD) methods, based on Cartesian or cylindrical coordinate systems, have certain limitations regarding irregular geometries [9], such as the geometry of a jet cross section, which is connected to a channel. Methods based on the body-fitted grid or the non-orthogonal grid systems do not have such limitations, and hence, in the present work, the body-fitted multi-block grid is used. The GAMBIT software [10] is employed to create the present complex geometry and then to generate the appropriate mesh. Four structured mesh sizes (hexahedral elements) are used to verify the independence of present numerical solution from the mesh size. The optimum grid size for various plates is chosen as follows: inlet region ($30 \times 20$), skin ($222 \times 30$) and outlet region ($60 \times 30$). Finally, the total of 9,060 mesh size is applied throughout the present work. Figure 3 represents a typical mesh generated around and within an outlet region shown in the present computational domain (see Figure 4).

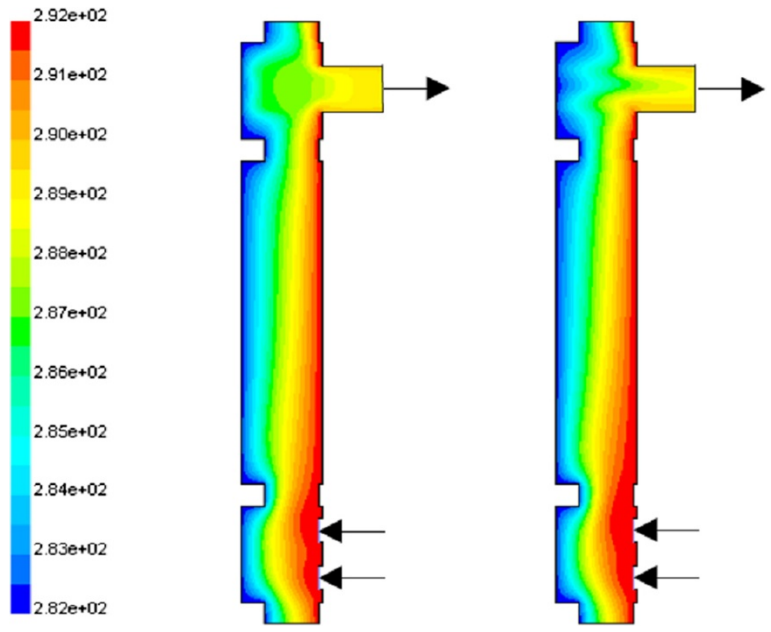


**Figure 6** Temperature distribution in the airflow window.

## Numerical details

The RANS and turbulence transport equations are solved numerically using the FLUENT code [11], which has been extensively validated against experimental data for many flow cases. The present numerical solution employs the finite volume-based finite difference approach [12,13], and it includes the following details: (1) Solution of the governing equations on the basis of three-dimensional Cartesian coordinates with adaptive, variable density grids is employed. (2) The second-order upwind scheme is used to discretize the convection terms. (3) The SIMPLE algorithm [12,13] is employed to correct the pressure term. (4) The ($k$-$\epsilon$/RNG) turbulence model is used. (5) The mixing is considered as a non-reacting flow. (6) The value of $1 \times 10^{-8}$ is considered as the convergence criterion for the energy equation, and $1 \times 10^{-6}$ for the other equations.

## Boundary conditions

The present computational domain, as illustrated in Figure 5, has five boundaries: two mass flow inlet for the airflow window and an outlet pressure plane for the outflow, two walls for the top and bottom of the airflow windows, a hot wall at the right-hand side of the airflow

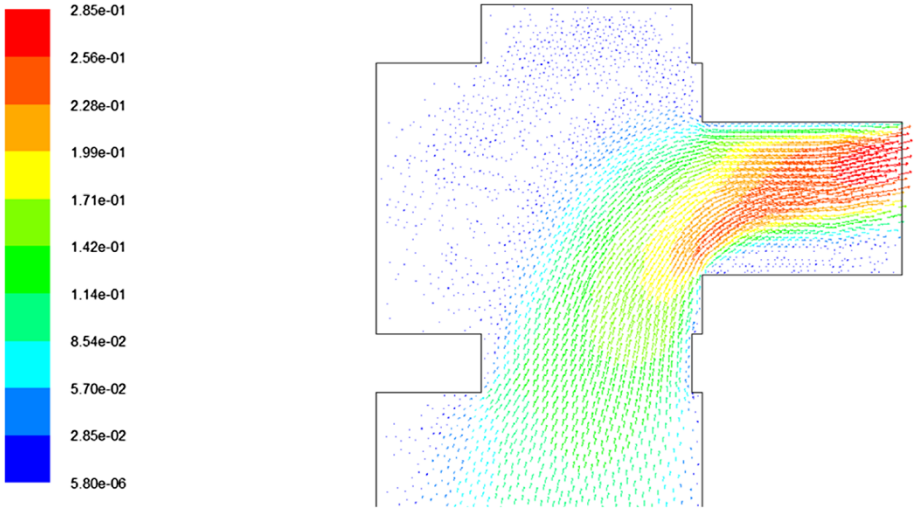


**Figure 7** Velocity vectors just passing the upper frame (present simulation).

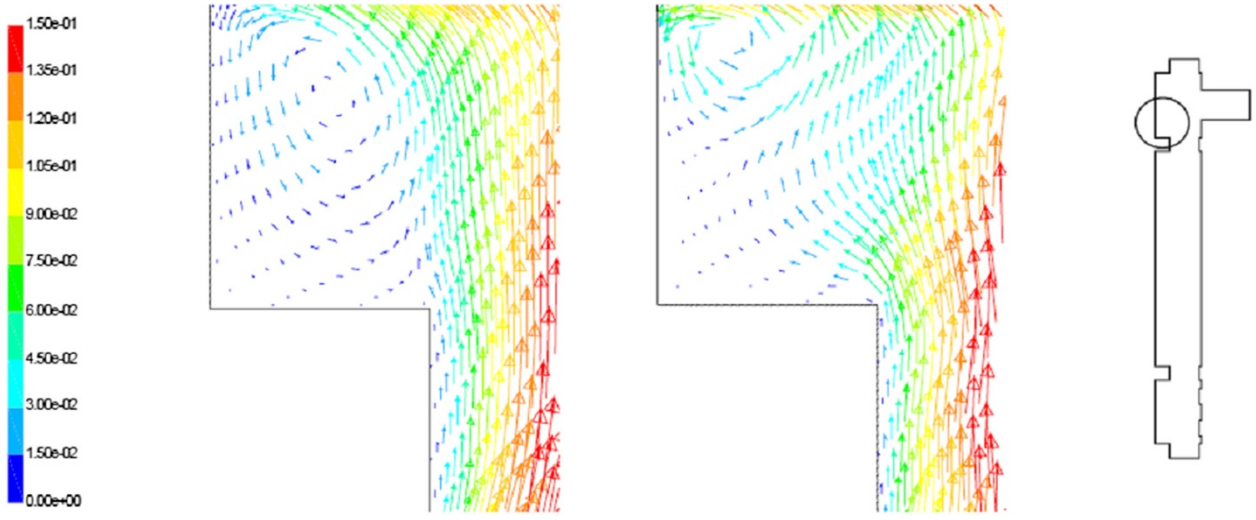


**Figure 8** Velocity vectors just passing the upper frame.

window and a hot wall at the left-hand side of the airflow window. At the inlet boundaries, uniform profiles of velocity and temperature are specified from the experimental data [4], where the relevant boundary conditions are taken as follows:

Inlet vent: $\underline{G}_i = 110\ m^3/h$
Hot wall: $T_H = 292.15\ K$
Cold wall: $T_C = 282.15\ K$

The turbulence intensity of inlet and length measure 0.1% and 10 mm, respectively. At the outlet region, sufficiently far from the inlet vent, a pressure outlet is considered. The walls (including top and bottom walls) are all considered as adiabatic; the walls (including right and left walls) are all considered as constant temperature.

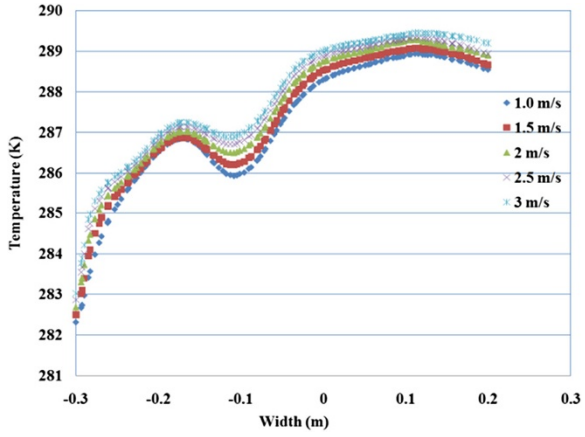


**Figure 9** Temperature variations in relation to airflow window width for different velocity.

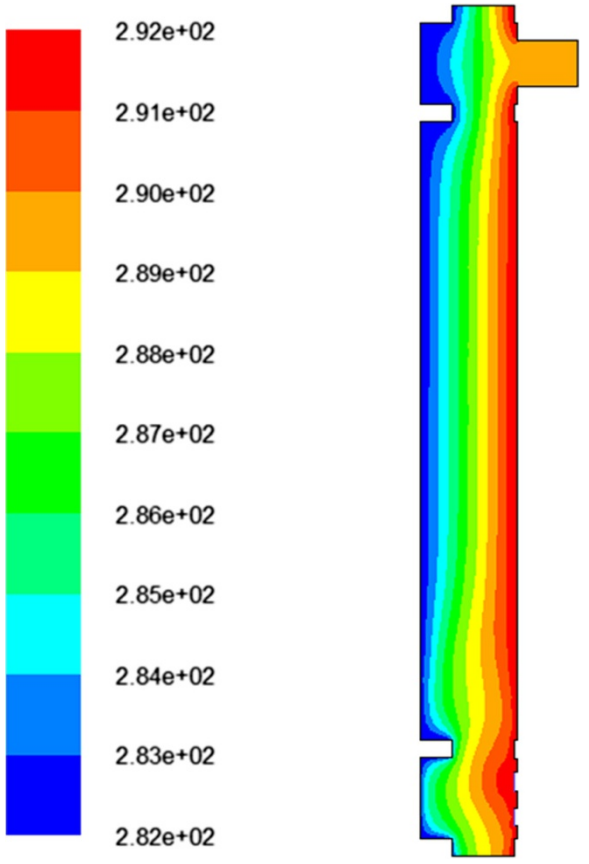


**Figure 10** Temperature distribution in the airflow window for free convection.

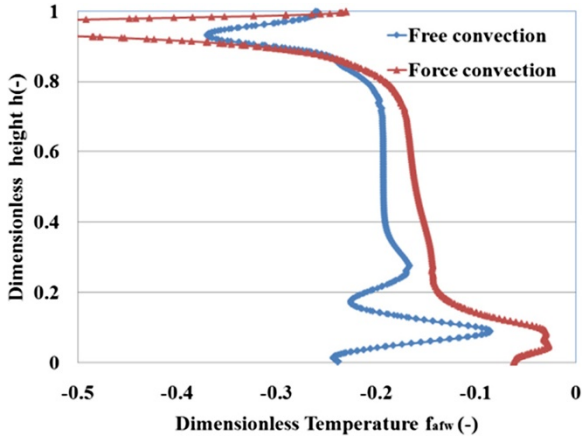


**Figure 11** Cavity air vertical dimensionless temperature profile in the airflow window for free and forced convection.

### Adiabatic effectiveness

The influence of the airflow rate on the vertical temperature difference in the airflow windows is illustrated, and it is defined as follows [4]:

$$f_{\mathrm{afw}} = \frac{T_{\mathrm{x}} - T_{\mathrm{i}}}{T_{\mathrm{i}} - T_{\mathrm{e}}} \tag{9}$$

where $T_{\mathrm{x}}$ is the temperature at height x, and $T_{\mathrm{e}}$ and $T_{\mathrm{i}}$ are the exterior and interior temperature (in degree Celsius). The results on $f_{\mathrm{afw}}$ are presented for the middle jet hole (center-line plane) in a row, in the case of film cooling technique only.

## Results and discussion

Figures 5 and 6 represent the temperature distribution in the airflow window, and a comparison is made between the present numerical results and the available experimental data of Baker et al. [4]. Figures 7 and 8 represent the velocity vectors just passing the upper frame in the airflow window, and a comparison is made between the present numerical results and the available experimental data of Baker et al. [4]. There exists a reasonably good agreement, and hence, the present numerical solution may also be used for the other analysis.

Figure 9 illustrates the typical temperature variations in relation to airflow window width for different velocity inlet adjacent outlet region. It can be seen that the temperature variations increased with velocity; also, the maximum temperature occurs near the outlet region because of the existent hot wall.

Figure 10 represents the temperature distribution in the airflow window for free convection simulation. It can be seen that the temperature is uniform near the walls, compared to forced convection simulation.

The influence of the airflow rate on the vertical temperature difference in the airflow windows for forced and free convection heat transfer is illustrated in Figure 11. It can be seen that in free convection, the airflow rate is higher compared to forced convection.

The dynamic pressure on the vertical temperature difference in the airflow windows for the forced and free convection heat transfer is illustrated in Figure 12. It can be seen that in free convection, the airflow rate is higher compared to the forced convection.

Figure 13 illustrates the influence of the airflow rate on the vertical temperature difference in the airflow

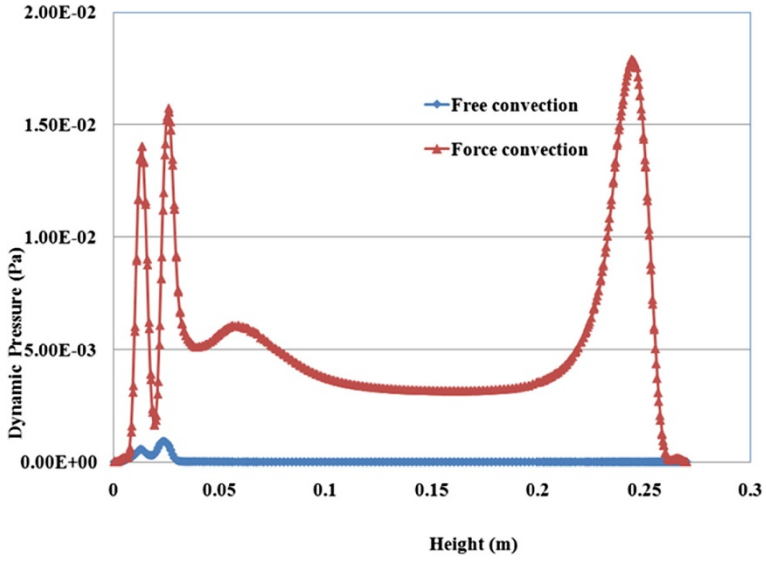


**Figure 12** Cavity air dynamic pressure versus height in the airflow window for free and forced convection.

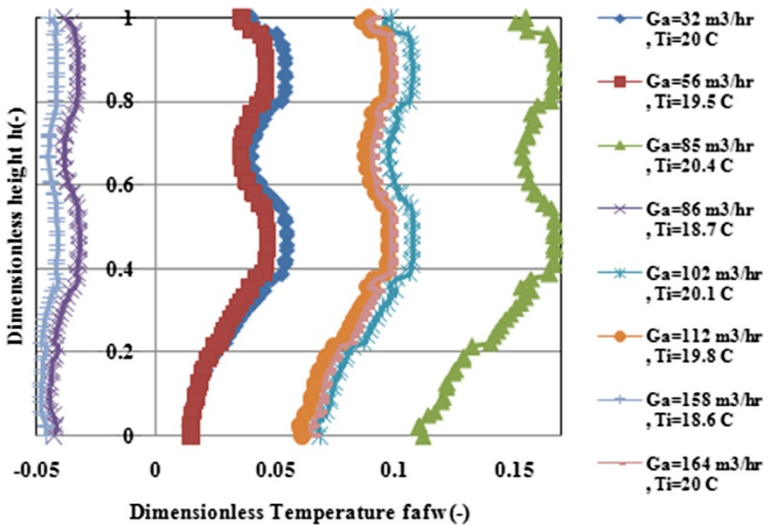


**Figure 13** Cavity air vertical dimensionless temperature profile in the airflow window for different airflow rates.

windows for different airflow rates with similar solar radiation. Based on Figure 12, we can assume that the airflow rate in the exterior cavity is lower than in the interior cavity since (1) the vertical temperature gradient is higher, indicating that the air has more time to heat up while flowing through the exterior cavity, and (2) the outlet temperature trends more towards the temperature at the top of the interior cavity, which indicates that a higher amount of air from the interior cavity flows towards the outlet region.

Figure 14 illustrates the influence of the airflow rate on the vertical temperature difference in the airflow windows for different cavity widths. It can be seen that airflow influence is not proportional to width such that it has an optimum amount at 300 mm.

Figures 15 and 16 represent the streamline in the airflow window for forced and free convection simulations. It can be seen that the streamline in forced convection is uniform streamline compared to free convection. However, free convection has more rotation stream line due to high bouncy force.

## Conclusions

Overall forced convective heat transfer in an airflow window was calculated using a CFD code and

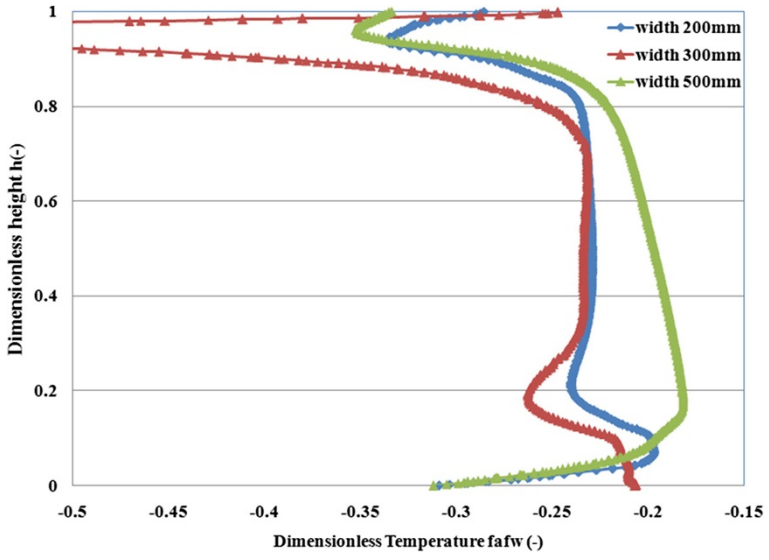


**Figure 14** Cavity air vertical dimensionless temperature profile in the airflow window for different cavity widths.

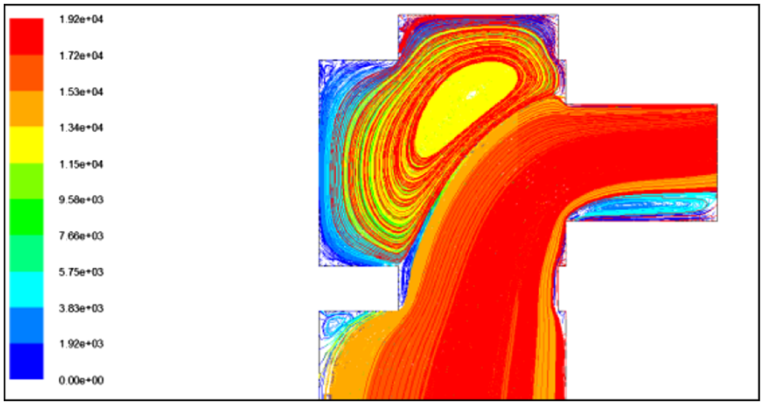


**Figure 15** Variations of streamline in forced convection.

compared with correlations based mainly on experimental results. The main conclusions may be drawn as follows:

1. A comparison between the present numerical results with the available experimental data is made. There exists a reasonably good agreement, and hence, the present numerical solution may also be used for the energy technique analyses.
2. A comparison between forced convection and free convection results illustrates that airflow influence increases in airflow windows.
3. Comparatively, it can be said that the effect of airflow in airflow window is proportional to inlet temperate and flow rate, but the effect of temperate is higher than the effect of flow rate.
4. Airflow influence in airflow window is not proportional to airflow window width and has an optimum amount at 300 mm.
5. By comparing streamline in forced and free convections, it can be said that streamline in forced convection behaves uniformly and regularly.
6. Effect of turbulence modeling is important, and comparing numerical and experimental results provides an acceptable and reasonably good agreement.

**Abbreviations**

*f*: dimensionless temperature (–); *H*: cavity height (m); *h*: convective heat transfer coefficient (W/m$^2$ K); $G_\alpha$: airflow rate (m$^3$/s); *V*: velocity (m/s); *w*: cavity width (m); α: thermal diffusivity (W/m K); $T_i$: inlet temperature (K); $T_C$: cold wall temperature (K); $T_H$: hot wall temperature (K).

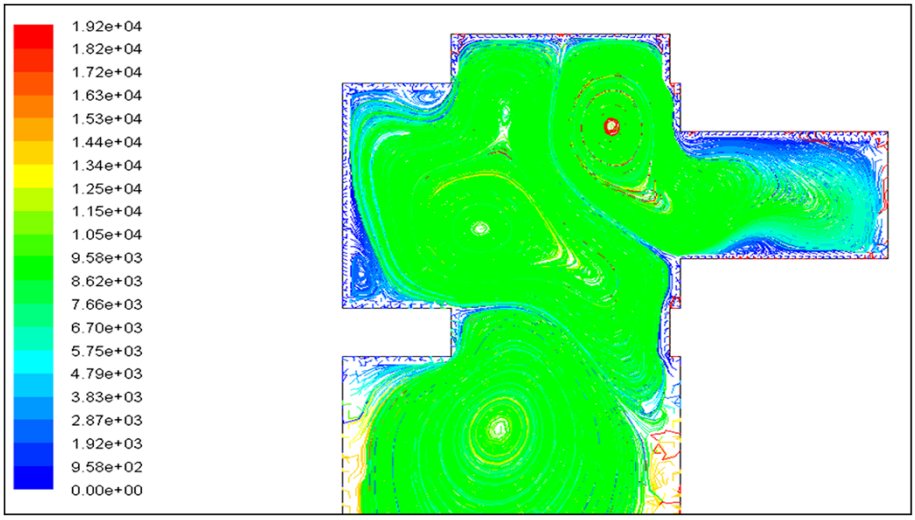


**Figure 16** Variations of streamline in free convection.

**Competing interests**
The authors declare that they have no competing interests.

**Authors' contributions**
MG collected the airflow window data. Modeling and product mesh were created by MG and MAB. MG carried out computations and analysis. MAB and MG drafted the manuscript. All authors read, edited and eventually approved the final manuscript to be submitted.

**Acknowledgments**
The support from the Department of Energy Engineering, Science and Research Branch, Islamic Azad University, Tehran, Iran, is gratefully acknowledged.

**Author details**
[1]Department of Energy Engineering, Science and Research Branch, Islamic Azad University, P.O. Box 147789385, Tehran, Iran. [2]Department of Chemical Engineering, Tehran University, P.O. Box 147789385, Tehran, Iran. [3]Department of Energy System Engineering, Islamic Azad University of South Tehran Branch, P.O. Box 189, Tehran, Iran. [4]Department of Mechanical Engineering, Islamic Azad University of Roudehen branch, P.O. Box 189, Tehran, Iran.

Received: 19 April 2012 Accepted: 21 May 2012
Published: 20 August 2012

**References**

1. Brandle, K, Boehm, RF: Airflow windows: performance and applications, Proceedings of the ASHRAE/DOE conference, pp. 361–379. Thermal Performance of the Exterior Envelopes of the Building II, Clearwater Beach (1982)
2. Ripatti, H: Airflow window system – Making the fenestration the solution rather than the problem in energy use. Proceedings of the ASHRAE Winter meeting, Atlanta (1984)
3. Park, SD, Suh, HS, Cho, SH: The Analysis of Thermal Performance in an Airflow Window System Model, Proceedings of the ASHRAE/DOE/BTECC/CIBSE Conference, pp. 361–375. Thermal Performances of the Exterior Envelopes of Buildings IV, Clearwater Beach (1989)
4. Baker, P, Saelens, D, Grace, M, Inoue, T: Advanced Envelopes – Methodology, Evaluation and Design Tools. Acco, Leuven (2000). Annex 32, Final report
5. Ziller, C: Modellversuche und Berechnungen zur Optimierung der natürlichen Lüftung durch Doppelfassaden (in German). Ph.D. Thesis. Shaker Verlag, Aachen (1990)
6. Busselen, B, Mattelaer, P: Experimental evaluatie van actieve gevelsystemen in het Vliet proefgebouw (in Dutch). MSc thesis, Laboratory for Building Physics. KU Leuven, (2000)
7. Wilcox, DC: Turbulence Modeling for CFD. DCV Industries, Inc, La Canada (1993)
8. Saelens, D, Hens, H: Low-energy design and airflow windows. Some considerations illustrated with a Case Study. Proceedings of the 10th International Symposium for Building Physics, International Building Physics Conference, September, pp. 27–29., Dresden (1999)
9. Versteeg, HK, Malalaskera, W: An Introduction to Computational Fluid Dynamics. The Finite Volume Method., McGraw-Hill, New York (1960)
10. GAMBIT: User's Manual, Version 1.1.2. Vol **2**., Anon, Lebanon, USA (1998)
11. FLUENT: *User's Manual, Version 1.1.2*, Vol **2**., Anon, Lebanon, USA (1998)
12. Patankar, SV: Numerical Heat transfer and Fluid Flow. MacGraw-Hill, New York (1980)
13. Cebeci, T, Shao, JP, Kafyeke, F, Laurendeau, E: Computational Fluid Dynamics for Engineers. Horizons Publishing Inc, Long Beach (2005)

doi:10.1186/2251-6832-3-14
**Cite this article as:** Ghadimi *et al.*: Analysis of free and forced convection in airflow windows using numerical simulation of heat transfer. *International Journal of Energy and Environmental Engineering* 2012 **3**:14.